Determination of the transport lifetime limiting scattering rate in InSb/Al_xIn_{1-x} Sb quantum wells using optical surface microscopy

CrossMark

Christopher J. McIndo[a,*], David G. Hayes[a], Andreas Papageorgiou[a], Laura A. Hanks[a,1], George V. Smith[a], Craig P. Allford[a], Shiyong Zhang[b], Edmund M. Clarke[b], Philip D. Buckle[a]

[a] School of Physics and Astronomy, Cardiff University, Queen's Buildings, The Parade, Cardiff CF24 3AA, United Kingdom
[b] EPSRC National Centre for III-V Technologies, North Campus, University of Sheffield, Sheffield S3 7HQ, United Kingdom

ARTICLE INFO

ABSTRACT

We report magnetotransport measurements of InSb/$Al_{1-x}In_xSb$ quantum well structures at low temperature (3 K), with evidence for 3 characteristic regimes of electron carrier density and mobility. We observe characteristic surface structure using differential interference contrast DIC (Nomarski) optical imaging, and through use of image analysis techniques, we are able to extract a representative average grain feature size for this surface structure. From this we deduce a limiting low temperature scattering mechanism not previously incorporated in transport lifetime modelling of this system, with this improved model giving strong agreement with standard low temperature Hall measurements. We have demonstrated that the mobility in such a material is critically limited by quality from the buffer layer growth, as opposed to fundamental material scattering mechanisms. This suggests that the material has immense potential for mobility improvement over that reported to date.

1. Introduction

Indium antimonide (InSb) exhibits the lowest reported electron effective mass ($m^* = 0.014\ m_e$) [1] and highest reported room-temperature electron mobility ($\mu_e = 78,000\ cm^2\ V^{-1}\ s^{-1}$) [1] of any compound semiconductor. These properties make InSb particularly suited to many electronic applications including low power high frequency electronics and quantum device realisation. There has been a recent resurgence of interest in the development of high quality InSb material following the report of two-dimensional electron gas (2DEG) channel mobilities in excess of 200,000 $cm^2\ V^{-1}\ s^{-1}$ at $T = 1.8\ K$ [2–5], and the possibility of Majorana fermion observation in InSb nanowires [6,7].

Furthermore, the strong spin-orbit interaction and extremely large Landé g-factor ($g \approx -50$) [1,8] exhibited in InSb has gained attention for potential exploitation in spintronics and quantum information control [9–11].

Previous studies of carrier transport in InSb 2DEGs [3,4] have considered standard scattering mechanisms using the relaxation time approximation and described the mobility variation over a wide range of temperature (typically 3–293 K). Whilst there has been good agreement, parameters used have tended to be extreme values to enable acceptable fits to data. It is believed that a major scattering mechanism associated with material quality has not been considered previously, with this having a major effect on the mobility behaviour. Considering this additional structural scattering allows for far more reasonable values for standard scattering mechanisms, showing that there is immense potential for mobility improvement in this material.

2. Growth and sample details

The InSb quantum well heterostructures studied were grown by solid source molecular beam epitaxy (MBE) on semi-insulating GaAs substrates (and so are therefore lattice mismatched with regard to the substrate). In growth order, the epitaxy comprises an aluminium antimonide (AlSb) accommodation layer, a 3 μm $Al_{0.1}In_{0.9}Sb$ strain-relieving barrier layer (to allow for mismatch relaxation), a 30 nm InSb quantum well layer and a 50 nm $Al_{0.15}In_{0.85}Sb$ top barrier layer. Tellurium (Te) δ-doping is introduced into the top barrier, 25 nm above the InSb quantum well (QW). Deliberate doping of the lower barrier is avoided in order to prevent any impurity donor atoms being carried forward on the growth plane which could significantly compromise the transport lifetime of carriers in the quantum well. Hall bar devices with an aspect ratio of 5:1 (nominally 200 μm×40 μm) were

---

* Corresponding author.
E-mail address: mcindocj@cardiff.ac.uk (C.J. McIndo).
[1] Present address: Physics Department, Lancaster University, Lancaster LA1 4YB, United Kingdom.
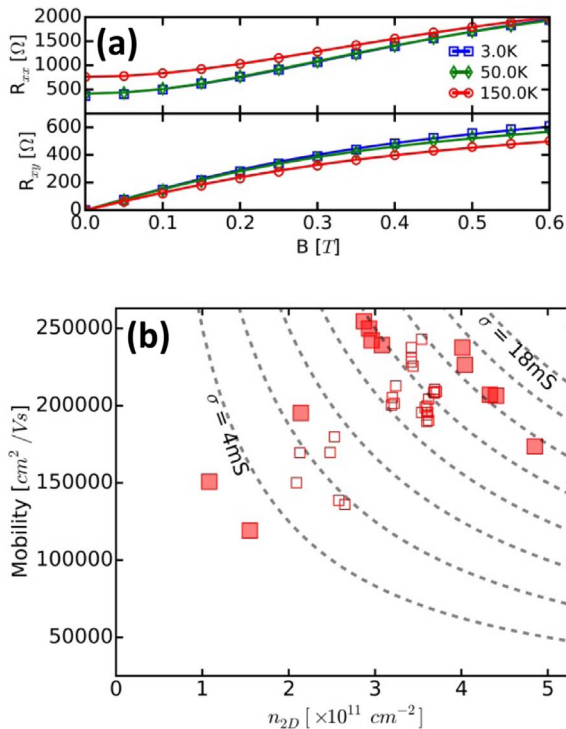
fabricated using standard photolithography, mesa wet etching and metal evaporation techniques. Relatively low temperature fabrication processes were used (≤100 ºC) to prevent excess metal penetration and tellurium dopant migration in the samples. The fabricated devices were mounted into non-magnetic ceramic leadless chip carriers and contact between the package and devices made via gold fine wire wedge bonding.

3. Experimental determination of mobility and sheet carrier density

All samples were measured over a range of temperature between 2.8 K and 300 K using a closed cycle pulse tube cryostat. The sample, when placed in the cryostat, was situated between the poles of a 0.6 T electromagnet. Electrical measurements of the samples were performed using a combination of a Keithley 6221 Current Source Meter and a Keithley 2401 Nanovoltmeter, using a pseudo-AC technique to remove any voltage drifts due to heating. To determine the mobility and carrier density, a constant current of either 1 μA or 2 μA was applied and the resulting transverse and longitudinal voltages recorded. No heating effects were observed with use of different current values. The magnetic field was then swept from 0 T to 0.6 T and from 0 T to − 0.6 T, and this was repeated as a function of temperature.

Fig. 1(a) shows the measured longitudinal (R_{xx}) and transverse Hall resistance (R_{xy}) for a typical sample at temperatures of 3 K, 50 K and 150 K. Also shown are 2 carrier fits to the data [12], with the fits matching well to the data. The fitting gives a 2D sheet carrier density (n_{2D}) of ~ 3×10^{11} cm^{-2} and mobility ~ 200,000 cm^2 V^{-1} s^{-1}, with n_{2D} increasing slightly over the temperature range studied.

Fig. 1(b) shows the extracted mobilities and carrier densities for a range of different samples at 3 K. Samples with increasing δ-doping (filled symbols) broadly define three regimes in the data. Initially, in

region 1, an increasing mobility is observed for an increase in carrier concentration n_{2D} (from 1×10^{11} cm^{-2} to 3×10^{11} cm^{-2}). This is believed to be due to single subband filling, calculated from Schrödinger-Poisson (S.P.) modelling [13], giving rise to increased Thomas-Fermi screening. The mobility, μ, then begins to plateau at ~ 250,000 cm^2 V^{-1} s^{-1} for a narrow range of carrier densities (region 2), before decreasing beyond 4×10^{11} cm^{-2} (region 3). In region 3, Schrödinger-Poisson modelling shows there is the possibility of multiple subband occupancy and additional intersubband scattering.
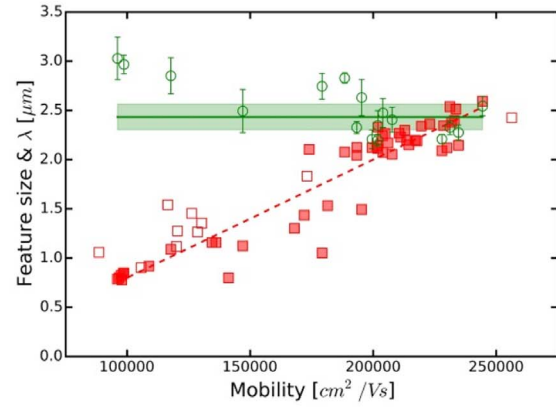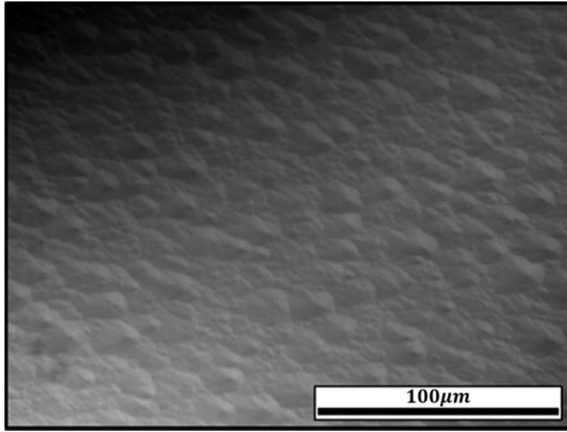
4. Nomarski image analysis

To help examine the limiting factors affecting the higher mobility samples, the surface morphology was considered using optical differential interference contrast DIC (Nomarski) imaging. To analyse the material surface multiple microscope images were taken of various samples in a spread of positions on the surface. Images were taken at an optical magnification of ×50. A raw Nomarski image of a standard wafer with n_{2D}~ 3×10^{11} cm^{-2} and μ~ 200,000 cm^2 V^{-1} s^{-1} is shown in Fig. 2.

The Nomarski image shows clear surface roughness, present similarly on all wafers imaged in this study. The roughness consists of approximately circular features with clear boundaries separating features. Due to the proximity of the 2DEG to the surface, it is reasonable to assume that this surface roughness, and in particular the boundaries, have a severe impact on the electron transport in the quantum well active layer.

Multiple grey scale images were taken of each wafer, and for each image, a small square sub-image was extracted using a window typically 200 pixels by 200 pixels of the original image. This ensured each sub-image contained many features. The sub-image was kernel smoothed to remove noise from the image and a 2D polynomial was fitted to remove any background trend (blush) in the image. To calculate the number of features, a 2D gradient was calculated by first determining gradients in the x and y directions, and depending on illumination, calculating the sum of or difference in these gradients. Any region above a set threshold was labelled as a definable feature and subsequently counted, giving the total number of features for the sub image. This analysis was repeated for multiple windows on each image (typically 40 sub images), with results combined to give a mean feature count, the error given by the standard deviation. This process was repeated for all images of each wafer, and corresponding feature counts averaged with errors combined in quadrature.

To turn the feature count into an average feature size, it was assumed that the features filled all space, and therefore the average area of each feature was given by the area of the sub-image divided by the mean feature count. A comparison of the mean feature diameter calculated using this Nomarski imaging analysis to the mean free paths, λ, deduced from a basic Drude transport model, is shown in Fig. 2. The mean free paths are calculated using mobilities from standard 3 K Hall measurements of samples shown in Fig. 1, as well as from historical samples from references [3,4,14,15].

There is a clear trend in measured mean free path with mobility, reaching a peak mean free path of ~ 2.5 μm. Fig. 2 shows the calculated feature diameter is approximately constant across all samples measured, with a mean value of ~2.43 ± 0.13 μm. This is in excellent agreement with the maximum mean free path deduced from mobility measurement, and is strongly suggestive that at low temperatures, when phonon effects are reduced, an electron traveling in the quantum well may travel ballistically through a feature until it reaches a boundary, causing a scattering event and ultimately limiting the transport lifetime. It is speculated therefore that the surface features are the low temperature limiting scattering mechanism in determining high electron mobilities in the QW. Further advancement in mobility and mean free path without significant buffer redesign will be impossible.

Fig. 1. (a) Typical longitudinal (R_{xx}) and Hall (R_{xy}) resistance vs. *B*-field for 3 K, 50 K and 150 K (symbols, every 25th data point plotted for clarity) with 2 carrier fits shown as solid lines [12]. (b) Measured mobility (two carrier fit) vs. 2D sheet carrier density (n_{2D}) from 3 K Hall measurements. A series of samples with increasing δ-doping levels is shown by the larger, filed symbols, showing at first an increasing mobility with carrier density. This then plateaus before then decreasing. Smaller, unfilled symbols indicate samples from other growth batches. Dashed lines are contours of constant conductance.

Fig. 2. Left: Optical Nomarski image of wafer surface, magnification × 50, for a sample with n_{2D} ~ 3×10^{11} cm^{-2} and mobility ~200,000 cm^2 V^{-1} s^{-1}. The surface is clearly textured, with features of varying sizes. Right: Comparison of mean feature diameter (and error) (open green circles) with weighted mean and one standard deviation (green line and shading) as a function of mobility, and measured mean free path (red squares) with linear regression fitted (dashed line). Filled squares represent samples from material measured in this paper, open squares represent historical samples taken from references [3,4,14,15] (For interpretation of the references to color in this figure legend, the reader is referred to the web version of this article.).

5. Transport lifetime model

To investigate the effect of the surface features on electron transport, a transport lifetime model was implemented following closely that performed by Orr et al. in their work on similar InSb QW devices [4]. The aim of this was to emphasise the effect of feature sizes acting as a limiting scattering mechanism in the low temperature, high mobility regime. This model includes several of the dominant scattering mechanisms present in III-V heterostructures, including ionised impurities (remote ionised scattering from dopant ions and background *p*-type impurity scattering), phonons (both optical and acoustic phonons) and interface roughness. Also included is the effect of band non-parabolicity in the form of a modified effective mass, deduced from a six-band Kane model [3,15,16]. The equations and parameters used for this transport model are taken from reference [4].

Included in the transport model is the effect of dopant dragging in the top cap. The scattering rate due to remote ionised impurities is now an extended sum of scattering from each individual 2D sheet of dopant charge, added inversely using Mathieson's rule. The charge density in each sheet follows an exponential drop off, with the total amount of charge being the sum of all sheets. This results in a slight reduction of scattering compared to a perfect single *δ*-plane with the same amount of dopant. In this system, it is assumed that the dopant atoms are fully ionized, however not all of the electrons are donated to the well, with a proportion instead transferring to the surface. This proportion is taken as another exponential drop off, steeper than that of the dopant distribution. This ratio of dopant donating electrons to the well vs. total dopant atoms is necessary to achieve correct Schrödinger-Poisson models (where ratios of ~5 to ~6 were needed to achieve the correct sheet carrier densities) and so this ratio is included the transport model studied here. To match the modelled mobility to the measured mobility, physical parameters for each sample were considered. These included sheet carrier density at 3 K, various interface rms roughness values and background concentrations, as well as the ratio of dopant activated into the well. It was found that for reasonable values of background *p*-type impurities (~1−10×10^{15} cm^{-3}) and rms roughness 0−5 monolayers), activation ratios significantly greater than those predicted by S.P. modelling were required. To achieve more reasonable ratios and to explain the measured mobility, another scattering mechanism is needed [17].

The model can be adapted to include an extra scattering rate term corresponding to the dimensions of the physical surface features observed in Nomarski imaging. If these features are taken as the ballistic mean free path length (l_e), with inelastic scattering occurring at

the boundaries, then their corresponding scattering rate is given by:

$$\frac{1}{\tau_l} = \left(\frac{l_e}{\sqrt{n_{2D}}}\right)\left(\frac{hm^*}{e^2\sqrt{2\pi}}\right)^{-1} \tag{1}$$

where n_{2D} is the 2DEG sheet carrier density in the QW [4].

A typical graph of the modelled temperature dependant mobility, including a non-parabolic effective mass, is shown in Fig. 3 alongside data for a sample with a 3 K mobility of approximately 200,000 cm^2 V^{-1} s^{-1}. The model matches the data well in the low temperature regime where the dominant scattering mechanism is associated with the surface features. The proposed scattering mechanism is only observed at low temperatures whereas high temperature effects are dominated by phonon scattering.

Performing this analysis for all of the measured samples using a typical feature size of 2.4 μm and a reasonable background dopant concentration of $p = 5\times10^{15}$ cm^{-3}, the modelled and measured mobilities are in close agreement at low temperatures. The required ratios of total dopant to carriers in the well are generally around 0−10 for the higher doped, high mobility samples, matching those required for the S.P. modelling. This strongly suggests that scattering due to surface feature boundaries is indeed a limiting scattering mechanism in these QW structures. For the more lightly doped, lower mobility
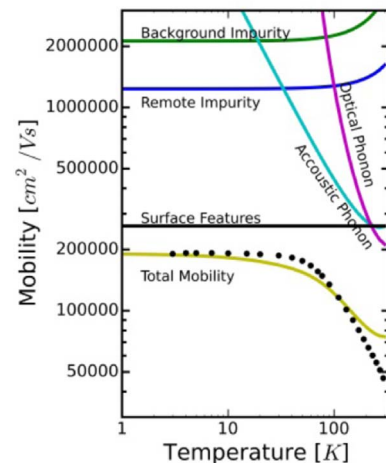
Fig. 3. Transport model mobility (lines) and measured data (symbols) vs. temperature including scattering due to 2.4 μm features as well as standard scattering terms (using typical values). The effect of dopant dragging on remote ionised impurity scattering is also included.

samples, the ratios required are slightly higher, indicating that physical feature scattering is not the limiting factor here, in agreement with the analysis in the Nomarski imaging section. Instead, in this regime, the remote ionised impurity scattering is dominating, with the subband filling and associated Thomas-Fermi screening leading to increased mobility with carrier density.

6. Conclusions

We have studied InSb/AlInSb QW 2DEG material and have shown evidence for three characteristic regimes in the measured low temperature Hall mobility behaviour with carrier density. We have demonstrated these regimes can be described by consideration of a combination of band filling from Schrödinger-Poisson modelling and physical surface structure scattering. Using image analysis techniques, representative feature sizes were extracted from Nomarski images of the material surfaces, with these shown to be a transport limiting scattering centre equal to the largest low temperature mean free paths measured. Through use of a conventional transport model, with updated terms for scattering due to a distribution of dopant, and for scattering due to physical features, we have shown it is possible to match predicted carrier densities and mobilities to those measured using low temperature Hall measurements. This work shows that with correct buffer redesign there is a clear potential for significant improvement in the mobility of such material, leading to many possible future implementations for high mobility materials.

Acknowledgements

References

[1] O. Madelung, U. Rössler, M. Schulz, Landolt and Bornstein - Group III Condensed matter: Group IV Elements, IV-IV and III-V Compounds. Part b - Electronic, Transport, Optical and Other Properties, Springer, 2002.

[2] W. Yi, et al., Gate-tunable high mobility remote-doped InSb/In$_{1-x}$Al$_x$Sb quantum well heterostructures, Appl. Phys. Lett. 106 (2015) 142103.

[3] O.J. Pooley, et al., Quantum well mobility and the effect of gate dielectrics in remote doped InSb/Al$_x$In$_{1-x}$Sb heterostructures, Semicond. Sci. Technol. 25 (2010) 125005.

[4] J.M.S. Orr, et al., Electronic transport in modulation-doped InSb quantum well heterostructures, Phys. Rev. B 77 (2008) 165334.

[5] F. Qu, et al., Quantized conductance and large g-factor anisotropy in InSb quantum point contacts, Nano Lett. 16 (2016) 7509–7513.

[6] V. Mourik, et al., Signatures of Majorana fermions in hybrid superconductor-semiconductor nanowire devices, Science 336 (2012) 1003–1007.

[7] M.T. Deng, et al., Anomalous zero-bias conductance peak in a Nb–InSb nanowire–Nb hybrid device, Nano Lett. 12 (2012) 6414–6419.

[8] B. Nedniyom, et al., Giant enhanced g-factors in an InSb two-dimensional gas, Phys. Rev. B 80 (2009) 125328.

[9] J.W.G. van den Berg, et al., Fast spin-orbit qubit in an indium antimonide nanowire, Phys. Rev. Lett. 110 (2013) 066806.

[10] R. Li, et al., Controlling a nanowire spin-orbit qubit via electric-dipole spin resonance, Phys. Rev. Lett. 111 (2013) 086805.

[11] D.D. Awschalom, et al., Quantum spintronics: engineering and manipulating atom-like spins in semiconductors, Science 339 (2013) 1174–1179. http://dx.doi.org/10.1126/science.1231364.

[12] M.A. Reed, et al., Investigation of parallel conduction in GaAs/Al$_x$Ga$_{1-x}$As modulation-doped structures in the quantum limit, IEEE . J. Quantum Electron. 22 (9) (1986) 1753–1759.

[13] I.-H. Tan, et al., A self-consistent solution of Schrödinger-Poisson equations using a nonuniform mesh, J. Appl. Phys. 68 (1990) 4071.

[14] O.J. Pooley, et al., Transport effects in remote-doped InSb/Al x In 1-x Sb heterostructures, New J. Phys. 12 (2010) 053022.

[15] A.M. Gilbertson, et al., Zero-field spin splitting and spin-dependent broadening in high-mobility InSb/Al$_x$In$_{1-x}$Sb asymmetric quantum well heterostructures, Phys. Rev. B 79 (2009) 235333.

[16] J.H. Davies, The Physics of Low-Dimensional Semiconductors, An Introduction, Cambridge University Press, 1998, p. 263.

[17] D. Jena, et al., Quantum and classical scattering times due to charged dislocations in an impure electron gas, Phys. Rev. B 66 (2002) 241307. http://dx.doi.org/10.1103/PhysRevB.66.241307.